Supporting Information

The reshaping role of GM1: membrane curvature and asymmetry in giant vesicles

Raktim Dasgupta[1,2], Markus S. Miettinen[1], Nico Fricke[1,3], Reinhard Lipowsky[1] and Rumiana Dimova[1,*]

[1] Department of Theory and Bio-Systems, Max Planck Institute of Colloids and Interfaces, Science Park Golm, 14424 Potsdam, Germany

[2] Current address: Laser Biomedical Applications Section, Raja Ramanna Centre for Advanced Technology, Indore-452013, India

[3] Current address: Department of Molecular Physiology and Biophysics, Vanderbilt University, School of Medicine, Nashville, Tennessee (TN)

*E-mail: dimova@mpikg.mpg.de

Text S1. Preparation of giant unilamellar vesicles (GUVs)

GUVs were grown using the electroformation technique (1). 1-palmitoyl-2-oleoyl-sn-glycero-3-phosphatidylcholine (POPC) and GM1 with varying concentration of up to 10 mol% were dissolved in a dichloromethane:methanol (2:1) solution to a concentration of 3.19 mM. Both lipids were purchased from Avanti Polar Lipids (Alabaster, AL). For fluorescence imaging of the vesicles, additionally 0.1 mol% Texas Red dihexadecanoyl-glycerophosphoethanolamine (TR-DHPE) or 0.1 mol% Bodipy FL C5-ganglioside GM1 (Bodipy-GM1) were added. 20 µl of the lipid solution was spread onto the electrically conductive sides of two indium-tin oxide (ITO)-coated glass plates (Delta technologies Lt.) heated to 50 ºC and dried under vacuum for two hours to remove the organic solvents. The glass plates were put against a 2 mm thick Teflon spacer to form a close chamber. 1 mM HEPES buffer (pH 7.4, 0.5 Na HEPES; Sigma-Aldrich, St. Louis, MO) was filled into the chamber and thereafter a sinusoidal AC electric field at 10 Hz was applied for electroswelling the lipid films. In the first phase of the electroswelling process, the amplitude of the applied field was linearly increased from 0.1 V (peak to peak) to 0.8 V (peak to peak) over 30 min. Thereafter the voltage was held steady for 60 min for growing the vesicles. Detachment of the formed vesicles from the glass surfaces was achieved by subsequent application of electric field with decreasing frequency down to 5 Hz over 20 minutes. All the voltages were

www.pnas.org/cgi/doi/10.1073/pnas.1722320115

measured at the ITO coated glass plates. Once the vesicles are formed, they were found to be stable and could be transferred to glass chambers used under microscopes for further investigations. Both the drying and electroswelling were carried out at 40 °C since at that temperature the lipid bilayer remains fluid and no phase separation occurs (2).

Text S2. Internal tubes generated upon dilution of vesicle suspensions

To understand the origin of the asymmetric distribution of GM1 across the membrane bilayer we carried out studies on the vesicles at different stages of preparation. The vesicle electroformation was performed under the confocal microscope while keeping the temperature of the solution constant at about 40 °C by placing the electroformation chamber in contact with a heat-flow chamber connected to a thermostat. Electroformed vesicles either attached to the glass substrate or floating were observed, but none of these could be seen with internal tubes (Fig. S1A). Since during electroformation the vesicle membrane tension remains high and this could be a likely reason for not observing any tubes, after electroformation, the vesicle suspension was transferred to a glass container and kept at room temperature overnight so that the vesicles could relax. Similar observations were made whereby only occasional vesicles could be found with internal tubes. The majority of the vesicles were free of tubes (Fig. S1B). Finally, the vesicle solution was diluted tenfold in a freshly prepared 1 mM HEPES buffer. Soon after that, a large number of vesicles with internal tubes could be seen (Fig. S1C). The observation suggests the important role of dilution of the vesicle external medium by vesicle-free buffer in the occurrence of the tubes.

To understand whether using HEPES as dilution medium is the key factor in the tube formation process, we also prepared vesicles in pure water. The observations were identical as with HEPES and shown in Fig. S1D,E. Minimal tube formation was observed until the original suspension medium was tenfold diluted by fresh water (Fig. S1E). This clearly suggests that the tube formation mechanism is independent of HEPES being used as suspension medium and dependent on the dilution of the concentration of GM1 in the surrounding medium of the prepared vesicles.

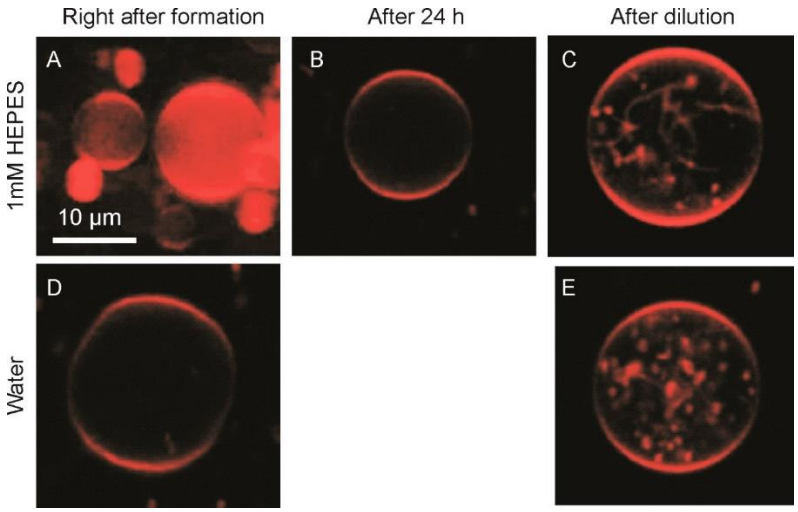

Figure S1. Vesicles observed at different stages of preparation in (A-C) 1 mM HEPES solution or (D, E) water. Internal tubes are observed only after the surrounding medium of the vesicles were diluted tenfold by fresh medium, i.e. HEPES buffer or water (C, E).

S3. Generation of external tubes upon external addition of GM1

The formation of internal nanotubes in the GM1 doped vesicles upon dilution of the external medium indicates desorption of GM1 from the outer leaflet leading to an asymmetric distribution of GM1 between the leaflets. To confirm this, we carried out the following experiment. In the diluted suspension of vesicles, when the internal nanotubes are formed, GM1 was added to the external medium to increase the concentration of GM1 in the outer leaflet by spontaneous insertion of the molecules at higher surrounding concentrations. A simple estimate for vesicles prepared with 4 mol% GM1 used in the total lipid mixture and assuming that all of the lipid and GM1 has been included either in the solution or in the form of vesicles, the total concentration of GM1 after dilution with fresh buffer comes out to be about 1.45×10^{-7} M. This concentration includes GM1 which is membrane-bound as well as dissolved in the medium. Taking half of the above concentration as the upper limit for GM1 present in the inner leaflet, we added ~0.73×10^{-7} M GM1 (6 µl of 1.28×10^{-5} M GM1 dissolved in dichloromethane/methanol (2:1) solution) from outside to adjust the concentration of GM1 in the exterior medium to be the same or higher. Leaving the vesicle solution open for about 10 minutes let the small amount of methanol/dichloromethane mixture (added with GM1) evaporate and thereafter observations were made on the vesicles. Although some vesicles appeared to be damaged because of the addition of methanol/dichloromethane mixture, a large fraction of undamaged vesicles were observed to

attain a balanced distribution of GM1 between the two leaflets as judging from their smooth appearance without any internal tubes. More interestingly, occasionally some vesicles even with long external tubes could be seen. The occurrence of external tubes indicates higher concentration of GM1 in the outer leaflet of these vesicles and presumably results from the inhomogeneous distribution of GM1 following the addition. Note that the addition of the same amount of GM1-free methanol/dichloromethane solution did not lead to suppression of the internal tubes, but only resulted in rupturing a fraction of the vesicles in the sample.

To perform a more direct monitoring of the tube suppression and external tube generation, we externally added GM1 to the diluted vesicle solution while observing individual vesicles under microscope. The vesicle suspension was placed in a rectangular well-shaped sample chamber, which is open at the top and having a cover slip at the bottom. To a vesicle sample of 200 µl, we added from the top 1 µl of 0.1 mg/ml GM1 (~65 µM) dissolved in methanol/dichloromethane. A large fraction of the vesicles was observed to be damaged by the organic solvent. However, we could observe some of the vesicles over time to directly monitor the changes after the addition of GM1. Figure S2 summarizes the results. After preparation and tenfold dilution, the vesicle exhibits a large number of internal tubes, Fig. S2A. The vesicle thereafter was continuously monitored to observe the morphological changes after addition of the GM1 solution outside very slowly. Figure S2B-D shows the time lapsed images at 2 minutes intervals. A gradual disappearance of the tubes could be seen with time after increasing the concentration of GM1 in the exterior medium. After a longer time, even the appearance of large external nanotubes could be observed, see Fig. S2E. The observation conclusively shows the dependence of GM1 distribution between the membrane leaflets proportionately related to the concentration of free GM1 in the surrounding medium.

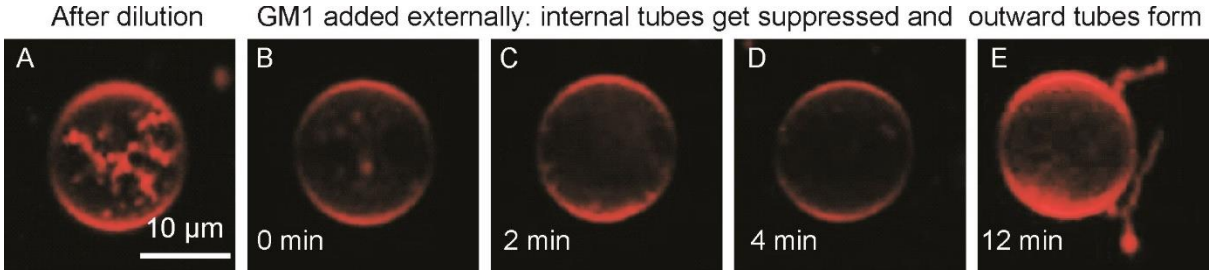

Fig. S2. Observations over a single vesicle with large number of internal tubes when subjected to addition of GM1 to the exterior medium. (A) Before adding GM1. (B-D) Images taken at 2-minute intervals showing the gradual disappearance of the tubes. (E) Around 12 min after the addition of GM1, the generation of large external tubes in the vesicle is observed.

S4. Electroporation of vesicles to measure the molar fractions of GM1 in the two membrane leaflets

For estimating the molar fractions of GM1 in membrane leaflets, first Alexa Fluor conjugated cholera subunit B (CTB-Alexa) was added to the vesicle solution at a concentration of 50 nM. Since the vesicles were intact, each CTB binds to five GM1 molecules present at the outer leaflet of vesicle membrane. After 10 min incubation, the vesicles were imaged under a confocal microscope (SP5 DMI 6000, Leica Microsystems Heidelberg GmbH, Germany) equipped with a 60 × HCX Plan APO objective (NA 0.75). Argon ion laser source at 495 nm was used to excite CTB-Alexa fluorescence. The bleaching of fluorescence over time was also monitored by time lapsed images of GUVs at intervals of 2 mins and no significant change could be seen for a total observation time of 30 min.

For pulse application, we used a modified electrofusion chamber (Eppendorf, Hamburg, Germany), which consists of a Teflon frame, a coverslip fixed at the bottom and a pair of parallel cylindrical electrodes with a radius of 92 μm and a separation of 0.5 mm fixed just above the bottom coverslip. Electric pulses of 50 ms duration and amplitudes ranging from 7 to 10 kV/m were applied directly under the microscope with a pulse generator (βtech, France). It has been previously reported that the critical poration potential depends on the initial membrane tension (3). Thus, the electroporation threshold can be different for each particular vesicle chosen depending on the initial tension. The pulse induces micron-sized pores in the vesicles and allows for inter-leaflet exchange of material as well as for CTB to access and bind to GM1 molecules in the inner leaflet of the vesicle membrane. After formation of large pores on the vesicles, a waiting period of ~10 minutes was allowed for CTB to bind to GM1 present in the inner membrane leaflet of the vesicles (see below and Fig. S3B).

The resulting increase in fluorescence can be used to assess the distribution of GM1 on both leaflets. We measured intensity line profiles across the membrane and along a circular path following the membrane contour as shown in Fig. S3A. While analyzing the porated vesicles, we left out the regions of the membrane with large number of outwardly hanging material as in the right panel of Fig. S3A. The time dependence of the fluorescence at the membrane is shown in Fig. S3B. It saturates already a couple of seconds after applying the electric pulse and stays constant during the pore lifetime suggesting that no unbinding of GM1 occurs.

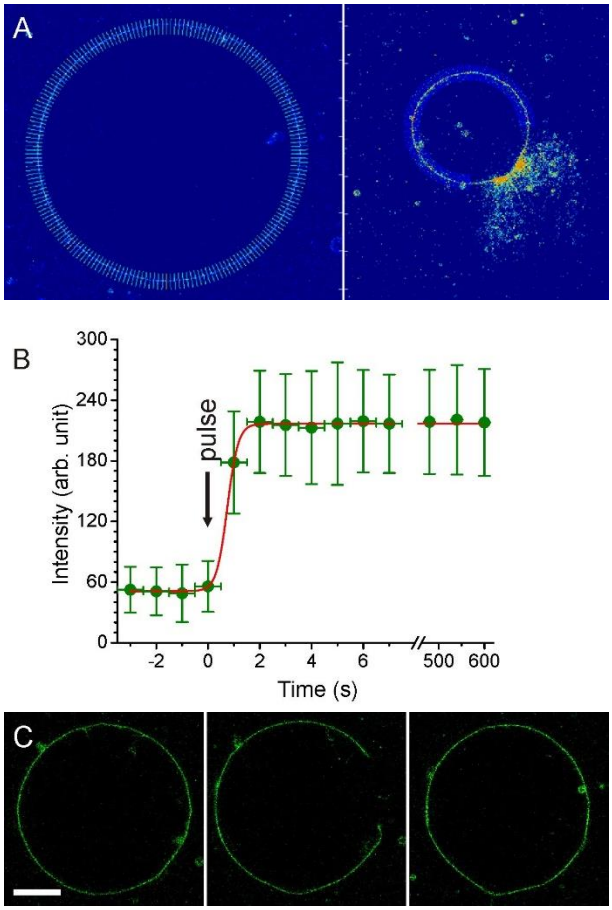

Fig. S3. Vesicle electroporation. (A) Image analysis to assess the GM1 distribution across leaflets. Two images (corresponding to those in Fig. 2A and 2C in the main text) and the lines along which the intensity line profiles following the membrane contours were acquired. The resulting intensity averages are displayed in Fig. 2D in the main text. (B) Time dependence of the membrane intensity before and during poration. The binding of CTB-Alexa to the membrane is saturated already in the first couple of seconds after opening the pore in the vesicle and stays constant until it closes (~10 min later). (C) Electroporation of a GUV with symmetric membrane. The vesicle exhibits no internal tubes which is an indication for spontaneous curvature close to zero. The confocal cross sections show the vesicle before (left), during (middle) and after (right) electroporation. Intensity profiles across the membrane (analyzed as explained in the main text) yield I_{after}/I_{before} = 1.8 for this vesicle. Scale bar, 25 μm.

As a control experiment, to confirm that the asymmetry is correctly represented by the ratio of membrane intensities before and after poration, I_{after}/I_{before}, we examined symmetric vesicles (presenting no tubes). One example (4 mol% GM1) is illustrated in Fig. S3C. On the average, we find I_{after}/I_{before} = 1.9 ± 0.4 (the error represents standard deviation from measurements on 6 vesicles from different batches). The proximity of the value of the intensity ratio to 2 confirms the validity of the approach.

The vesicle response to electric pulses was observed also under phase contrast at high acquisition speed (30 000 frames per second), Fig. S4.

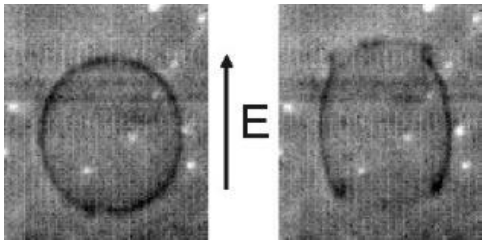

Fig. S4. A GUV (8 μm in diameter) exposed to a DC pulse (of field strength 1.5 kV/cm and duration 0.5 ms; the field direction is indicated with an arrow) exhibits large pores facing the electrodes as observed under phase contrast microscopy. At the pore rims, the membrane curls outward consistent with the negative spontaneous curvature resulting from the asymmetric GM1 distribution. The vesicles were prepared with 10 mol% GM1. The images before (left, 0 s) and at the end of the pulse (right, 0.5 ms) were acquired under phase contrast microscopy.

S5. Estimate for the GM1 concentrations on the inner and outer leaflets

After preparation, the vesicles are diluted tenfold unless otherwise specified (note that the degree of asymmetry depends both on the dilution as well as on the overall lipid concentration). After the dilution step, ϕ_{in} and ϕ_{out} are the molar fractions of GM1 in the inner and outer leaflets, respectively. With c_{in} and c_{out} we denote the molar concentrations of free GM1 inside and outside the vesicles, respectively. The partitioning equilibrium between bound and free GM1 is established on both sides of the membrane, therefore $\frac{\phi_{in}}{c_{in}} = \frac{\phi_{out}}{c_{out}}$. From the measurements on the change of CTB fluorescence intensity, we know that $\frac{\phi_{in}}{\phi_{out}} = \bar{I} \equiv \frac{I_{after}}{I_{before}} - 1$, leading to

$$c_{in} = \bar{I} c_{out} \tag{S1}$$

The dilution is done by mixing a small aliquot v (100 μl) from the prepared vesicle suspension with fresh (GM1-free) buffer to reach a total volume of V_t (1 ml). The volume of the electroformation chamber is V_{ch} (1.76 ml), of which the vesicles take a total volume of V_{ves}. The mass balance for GM1 in the diluted suspension gives

$$x\frac{n_{lip}}{2}(\phi_{in} + \phi_{out}) + xV_{ves}c_{in} + (V_t - xV_{ves})c_{out} = xn_{lip}\phi \quad , \tag{S2}$$

where $x = v/V_{ch}$, n_{lip} is the lipid molar equivalent used for the preparation of the GUVs ($n_{lip} = 6.38 \times 10^{-8}$mole) and ϕ is the mole fraction of GM1 (2 mol% or 4 mol%) used for the vesicle preparation. The first term in Eq. S2 represent the moles of GM1 bound to the membrane (inner and outer leaflets), while the second and third terms reflect the amount of free GM1 inside and outside the vesicles, respectively. Above, we have assumed that no lipid loss during the vesicle electroformation occurs.

Before the dilution step, GM1 is symmetrically distributed across the membrane, $\phi_{in}^0 \equiv \phi_{out}^0$ and $c_{in}^0 \equiv c_{out}^0$. Evidence for this symmetry is that no tubes are observed after the vesicle preparation, and even after 24 hours of equilibration. Since the membrane is impermeable to GM1, the surface and bulk concentrations of GM1 inside the vesicles remain unchanged after dilution and thus $\phi_{in} = \phi_{in}^0$ and $c_{in} = c_{in}^0$. This also implies that $c_{out}^0 = c_{in}$ and $\phi_{out}^0 = \phi_{in}$. Then, mass conservation for GM1 (before and after the dilution) in the external solution and leaflet implies

$$x\frac{n_{lip}}{2}\phi_{out} + (V_t - xV_{ves})c_{out} = x\frac{n_{lip}}{2}\phi_{in} + x(V_{ch} - V_{ves})c_{in} \quad , \qquad \text{(S3)}$$

where the right-hand side represents the initial amount of GM1 in the outer leaflet and in the medium corrected by the dilution factor. Assuming that the total amount of lipids is involved in forming vesicles of radius ~10 μm and taking for the molecular area of POPC ~68 Å^2 (4), and $n_{POPC} \cong n_{lip} = 6.38 \times 10^{-8}$mole, for the volume enclosed in the vesicles before the dilution we obtain $V_{ves} = 0.0436$ ml. This volume represents a negligible correction, $V_{ves} \ll V_{ch} < V_t/x$, and will be ignored. Inserting Eq. S1 in Eq. S2 gives

$$c_{out} = n_{lip}\frac{\phi - (\phi_{in} + \phi_{out})/2}{V_t/x + V_{ves}\bar{I}} \qquad \text{(S4)}$$

Introducing this expression in Eq. S3 and after some algebra, we obtain

$$\phi_{out} \cong \frac{\phi}{\bar{I}}\left[1 + \frac{xV_{ves}}{V_{ch}}(1 - \bar{I})\right] \qquad \text{(S5)}$$

The results for the two vesicle compositions used are shown in Table 1 in the main text.

S6. Optical tweezers and force measurement

The optical tweezers (5, 6) was built around a motorized inverted microscope (Axiovert 200M, Zeiss) and comprises of a single beam optical tweezers formed by focusing a

1064 nm, cw laser beam from a Nd:YAG laser (Spectra Physics, USA) through a 100×, NA 1.25 objective lens (Acroplan, Zeiss). Typical laser powers used were ~0.8 W at the sample. The microscope was equipped with a motorized stage (LStep13, Märzhäuser) that can be used to position and translate the sample chamber with a resolution of 50 nm and speed of 1-500 µm/s respectively. All measurements were performed at ~23°C. Images were captured by an EMCCD camera (ImagEM, Hamamatsu Corp) at 30 frames per second. ImageJ was used for size and coordinate analysis of vesicles using edge detection technique. The optical tweezers was used to trap latex microspheres (Polyscience Inc.) of 2 ± 0.045 µm diameter attached to the GUV membrane and therefore manipulating these to pull tubes. The tube pulling forces were estimated by monitoring the position shift of the trapped bead from the trap center, $f = -K_{trap}(x - x_0)$, where $x - x_0$ is the position shift of the trapped bead from the trap center (x_0) when a tube is pulled and K_{trap} is the stiffness of the trap. The calibration parameter K_{trap} was determined by drag-force method in which the motorized stage was used to drag a trapped bead through the chamber at several fixed velocities. During the stage movement, hydrodynamic forces act on the bead as $f_{drag} = 6\pi\eta R_{bead}U$, where η is the viscosity of the solution, R_{bead} is the radius of the bead and U is the velocity at which it is moved. The bead was imaged using the CCD camera and its position was determined using centroid tracking algorithm (7) written in MATLAB (Mathworks Inc). The precision of position sensing using the centroid tracking technique could be estimated to be ~4 nm and ~6 nm along *x* and *y* directions, respectively. All measurements were performed at a height of ~20 µm from the bottom glass boundary of the sample chamber. The stiffness of the tweezers was found to be ~88 pN/µm for typical laser power above the objective (at sample height) of 0.8 W. Once the stiffness was known, subsequent imaging and determining bead displacement allowed us to estimate the net tube pulling force acting on the bead by off-line analysis with a temporal resolution of ~ 33 ms.

S7. Micropipette manipulation of GUVs

For each experiment, a 5 mm wide, 15 mm long and 2 mm deep chamber was built by fixing one ~130 µm thick glass coverslip and 1 mm thick glass slide against each other separated by spacers. To prevent adhesion of the vesicles to the glass surfaces, the chamber and the micropipette were passivated by coating with 1 mg/ml BSA then rinsed with buffer containing 1 mM HEPES (pH 7.4). The chamber was mounted on the microscope and the vesicle solution was introduced. A single micropipette was inserted into the sample chamber

with the use of a three-dimensional micromanipulator system (Narishige Corp, Japan) clamped on the microscope. Following insertion, zero pressure across the pipette tip was attained and calibrated by watching the flow of small particles within the tip. Aspiration pressure was controlled through adjustments in the height of an attached mobile water reservoir mounted on a linear translational stage (M-531.PD; Physik Instrumente, Germany). This allowed for varying the membrane tension of the GUV from 1×10^{-6} to 3×10^{-4} N/m.

In order to obtain a projection length greater than the pipette radius at low aspiration pressures, vesicles with a low initial membrane tension were selected. For pulling inward tubes, first, a latex bead was trapped using the optical tweezers. Then, the aspirated vesicle was brought into contact with the bead and manipulated across the vesicle surface through the region opposite of the pipette. After that, the separation between the bead and vesicle membrane is increased to extend the tube to a suitable length (typically around 10 μm); this length was kept constant during the whole experiment. Membrane tension was then increased by steps. For each tension, the position of the bead relative to the trap center was recorded by video microscopy. For studying the spontaneous curvature of GM1, the waiting time between a pressure change and image acquisition was about 2 min in order to reach the equilibrium composition in the tube by lipid diffusion. This time scale is consistent with the time required for a lipid to explore a ~ 10 μm long membrane tube with a typical diffusion constant of 5 $\mu m^2/s$ (8). Before each set of experiments on a new vesicle, the zero reference pressure in the pipette was set by detecting the absence of movement of a bead in the pipette. For the experiments shown in Fig. 3E,F, the suction pressure of the pipette was changed from ~ 19.6 Pa to ~ 68.7 Pa, corresponding to changing heights of the water reservoir from 2 mm to 7 mm. The pressure change was typically done in five equal steps. The corresponding membrane tension could be estimated from Eq. 4 in the main text. All experiments were performed at room temperature, 23±1°C.

S8. Extruding inward and outward tubes from GM1-doped vesicles

For pulling an in-tube, a GUV was first held by the micropipette under very low aspiration pressure (~ 5 Pa) and thereafter taken into contact of a trapped latex bead. After allowing few minutes of contact between the latex bead and the membrane lipid, the GUV was slowly pressed to the trapped bead to cause it to bend the membrane inward and move inside of the vesicle via gradual wetting by the fluid membrane. The wetting of the trapped bead in the fluid membrane causes a natural adherence to occur between the lipid and the bead (9), and

thereafter, when increasing the separation between the bead and the vesicle membrane by translating the GUV further, an in-tube could be formed. The fluorescence from TR-DHPE could be used to image the membrane nanotube. A long sequence (one thousand frames) of bright-field images were recorded and therefore analyzed for measuring the position of the trapped bead to estimate the tube pulling force. The vesicle membrane tension could be subsequently set at higher values by applying higher suction pressure of the pipette and similar measurements were carried out to estimate the pulling forces. Afterwards, the vesicle membrane tension was reduced to a small value and the aspirated vesicle was moved in the opposite direction to manipulate the trapped bead towards the exterior of the vesicle. Subsequent increase in the separation between the vesicle and the bead cause the formation of an outward tube, on which similar measurements were carried out. During manipulation of the bead through the vesicle membrane, the mechanical tension over the membrane had to be reduced to a small value (typically ~ 0.01 mN/m) otherwise we observed that the bead can get dislodged out of the optical trap due to elastic forces of the membrane. The pulling force and the vesicle aspiration system were allowed to briefly equilibrate before initiating acquisition of images.

Figure S5 displays the difference between the force for pulling outward and inward tubes $f_{out} - f_{in} = -8\pi\kappa m$ on the same vesicle. Within the error, the force difference does not depend on the vesicle tension and can be used to deduce the membrane spontaneous curvature provided the bending rigidity is known or vice versa.

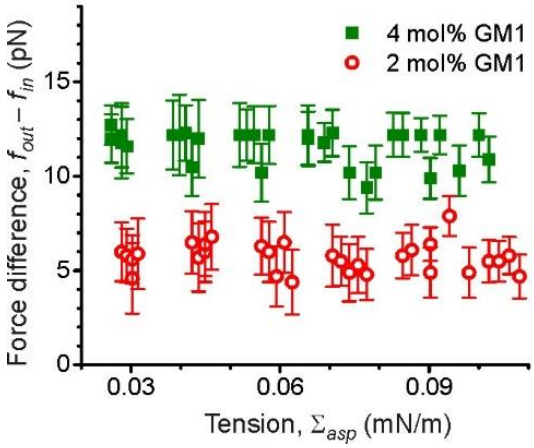

Fig. S5. Force difference $f_{out} - f_{in}$ for pulling outward and inward tubes on the same vesicle as a function of the membrane tension. The collected data is from 5 different vesicles for each membrane composition.

S9. Measuring the threshold tension at which tubes reform

In addition to tube pulling experiments performed to evaluate the threshold tension below which tubes spontaneously reform (black data in Fig. S6 assessed from $\Sigma_{asp}^{0} = 2\kappa m^2$), we measured this tension using micropipette aspiration and vesicle electrodeformation (2, 10), red data in Fig. S6. The latter methods were applied to explore membranes at higher concentration of GM1 and were thus performed at 40°C to avoid phase separation (2). All methods give consistent trend.

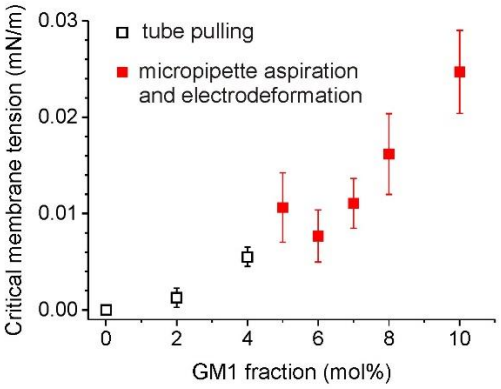

Fig. S6. Threshold membrane tension below which internal tubes reform into the vesicle body. For lower GM1 fractions (black squares), the data was collected from tube pulling experiments where the plotted critical tension corresponds to Σ_{asp}^{0} as assessed from the intercept of the data in Fig. 3F in the main text with the horizontal axis, see Eq. 8 in the main text. For higher GM1 fractions (red squares), the data was collected from micropipette aspiration and vesicle electrodeformation.

S10. Coarse-grained molecular dynamics simulations

We used the fast, flexible and free GROMACS (11-18) engine version 5.1.1 to run MARTINI (19) coarse-grained molecular dynamics simulations with the MARTINI-straight parameters (20). The GM1-containing POPC bilayers at full hydration, with sodium ions to obtain zero net charge, were simulated at 303 K and 1 bar. We first used the GM1 parameterization developed by López et al. (21), but observed strong clustering behavior of GM1 in this model, see Fig. S7A and Ref. (22). We thus built a new GM1 model by combining the bonded parameters of López et al. (21) with the non-bonded parameters of Gu et al. (22). This new model was free of the clustering artifact (see Fig. S7A), while maintaining the GM1 shape of the López model (Fig. S7B). Like the López model (Fig. S8B), it reproduced quantitatively our experimental data (Fig. 4 in the main text), while the

Gu model (22) did not. The lateral stress profiles of the bilayers were calculated with GROMACS-LS (23); only the Goetz-Lipowsky decomposition (24) could be used, as the Central Force Decomposition (25) diverges with the dihedral potentials present in the MARTINI GM1. The simulation box dimensions (*x*/*y*/*z*) were roughly 8 nm/8 nm/10 nm. The simulation lengths for the López model were 400 μs (except for the $\phi_{in} \mid \phi_{out} = 1|1$ system, 100 μs) with sampling rate of 500 ps. For our new model, the simulation length was 100 μs (except for the $\phi_{in} \mid \phi_{out} = 1 \mid 1$ system where it was 20 μs) with sampling rate of 100 ps. The number of independent samples for the standard error of the mean was determined by the blocking method (26). Due to the long-lived structural correlations caused by the GM1 clustering, in some of the simulations with the López model $\{\phi_{in} \mid \phi_{out} = 1|0; 2|0; 1|1; 9|1\}$ the blocking method failed to find a plateau spanning two orders of magnitude in time; for these systems the error was estimated by visually assessing the cumulative average.

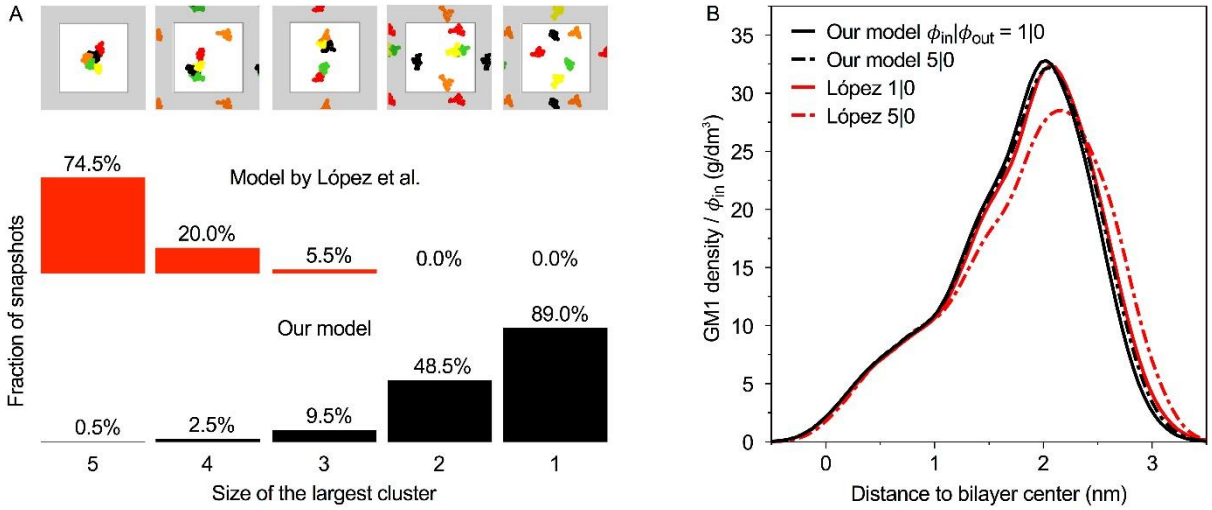

Fig S7. The two GM1 models examined here have drastically different GM1 clustering behavior. (A) Cluster size distributions observed in simulations with $\phi_{in} = 5; \phi_{out} = 0$. Snapshots categorized by the size of largest GM1 cluster: the top row shows an example for each category (each GM1 head group differently colored; view along the membrane normal; periodic images of the simulation box are shaded in gray). Fraction of snapshots of specific cluster size (cluster size 1 corresponds to non-clustered GM1) according to López et al. (21) and the model developed here. (B) The density profiles over the inner leaflet, normalized by the number of GM1s (ϕ_{in}), show that when alone ($\phi_{in} = 1$) the GM1 shapes in the two models were practically indistinguishable, and that clustering (seen for López $\phi_{in} = 5$, c.f. panel A) extended the GM1s slightly.

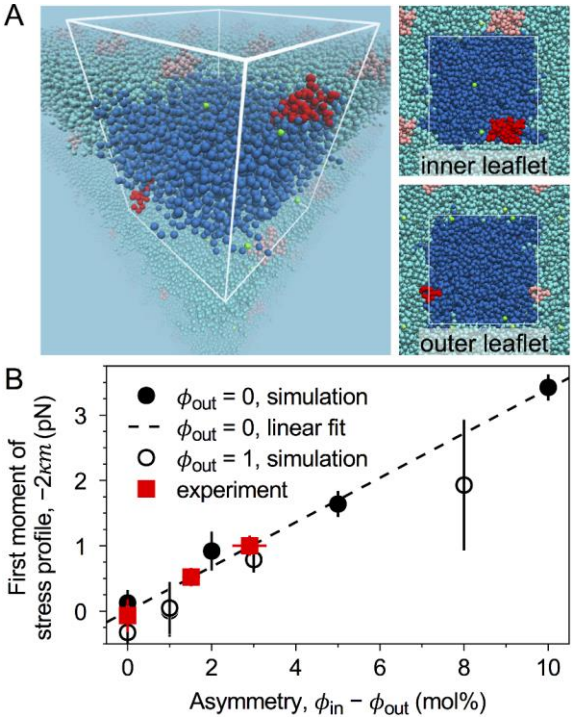

Fig S8. Simulation results for the GM1 model by López et al. (21) and comparison with experimental data from this work. (A) A simulation snapshot of the inner bilayer leaflet (upper monolayer within the white wireframe) and the outer leaflet (lower monolayer) for GM1 molar fractions $\phi_{in} = 4$ mol% and $\phi_{out} = 1$ mol% using the MARTINI coarse-grained molecular dynamics simulation model with GM1 parameters developed by López et al. (21). Leaflet-wise mole fractions directly indicate the numbers of lipids: $\phi_{in} = 4$ corresponds to 4 GM1 and 96 POPC molecules in the inner leaflet. The white wireframe with the strongly colored species (GM1 red, POPC blue, sodium green, water not shown) shows the simulation box, and the lightly colored molecules indicate its periodic images. (B) Comparison of simulation results to experiments. The first moment of the lateral stress profile ($-2\kappa m$) is plotted as a function of the bilayer asymmetry $\phi_{in} - \phi_{out}$ for bilayers when the outer leaflet is pure POPC ($\phi_{out} = 0$, solid circles), and when it contains one GM1 ($\phi_{out} = 1$, open circles). The dashed line represents the linear fit $-2\kappa m = 0.34(\phi_{in} - \phi_{out})$ to the data for $\phi_{out} = 0$. As for our model (see Fig. 4 in the main text), the dependence is quantitatively consistent with the experimental results (red squares) obtained from the pulling force for vanishing tension, see Eq. 9 in the main text.

References

1. Dimova R, *et al.* (2006) A practical guide to giant vesicles. Probing the membrane nanoregime via optical microscopy. *J. Phys.: Condens. Matter* 18(28):S1151-S1176.
2. Fricke N & Dimova R (2016) GM1 Softens POPC Membranes and Induces the Formation of Micron-Sized Domains. *Biophys. J.* 111(9):1935-1945.
3. Riske KA & Dimova R (2005) Electro-deformation and poration of giant vesicles viewed with high temporal resolution. *Biophys. J.* 88(2):1143-1155.

4. Kucerka N, Tristram-Nagle S, & Nagle JF (2005) Structure of fully hydrated fluid phase lipid bilayers with monounsaturated chains. *J. Membr. Biol.* 208(3):193-202.
5. Kraikivski P, Pouligny B, & Dimova R (2006) Implementing both short- and long-working-distance optical trappings into a commercial microscope. *Rev. Sci. Instrum.* 77(11):113703.
6. Dasgupta R & Dimova R (2014) Inward and outward membrane tubes pulled from giant vesicles. *J Phys D Appl Phys* 47(28):282001.
7. Dasgupta R, Verma RS, & Gupta PK (2012) Microfluidic sorting with blinking optical traps. *Opt. Lett.* 37(10):1739-1741.
8. Lipowsky R & Sackmann E (1995) *Structure and dynamics of membranes* (Elsevier Science, Amsterdam ; New York) pp v. <1A-1B, >.
9. Dietrich C, Angelova MI, & Pouligny B (1997) Adhesion of latex spheres to giant phospholipid vesicles: statics and dynamics. *J. Phys. II* 7(11):1651–1682.
10. Gracià RS, Bezlyepkina N, Knorr RL, Lipowsky R, & Dimova R (2010) Effect of cholesterol on the rigidity of saturated and unsaturated membranes: fluctuation and electrodeformation analysis of giant vesicles. *Soft Matter* 6(7):1472-1482.
11. Bekker H*, et al.* (1993) Gromacs - a Parallel Computer for Molecular-Dynamics Simulations. *Physics Computing '92*:252-256.
12. Berendsen HJC, Vanderspoel D, & Vandrunen R (1995) Gromacs - a Message-Passing Parallel Molecular-Dynamics Implementation. *Comput. Phys. Commun.* 91(1-3):43-56.
13. Lindahl E, Hess B, & van der Spoel D (2001) GROMACS 3.0: a package for molecular simulation and trajectory analysis. *J. Mol. Model.* 7(8):306-317.
14. Van der Spoel D*, et al.* (2005) GROMACS: Fast, flexible, and free. *J. Comput. Chem.* 26(16):1701-1718.
15. Hess B, Kutzner C, van der Spoel D, & Lindahl E (2008) GROMACS 4: Algorithms for highly efficient, load-balanced, and scalable molecular simulation. *Journal of Chemical Theory and Computation* 4(3):435-447.
16. Pronk S*, et al.* (2013) GROMACS 4.5: a high-throughput and highly parallel open source molecular simulation toolkit. *Bioinformatics* 29(7):845-854.
17. Pall S, Abraham MJ, Kutzner C, Hess B, & Lindahl E (2015) Tackling Exascale Software Challenges in Molecular Dynamics Simulations with GROMACS. *Lect Notes Comput Sc* 8759:3-27.
18. Abraham MJ*, et al.* (2015) GROMACS: High performance molecular simulations through multi-level parallelism from laptops to supercomputers. *SoftwareX* 1–2:19-25.
19. Marrink SJ, Risselada HJ, Yefimov S, Tieleman DP, & de Vries AH (2007) The MARTINI force field: Coarse grained model for biomolecular simulations. *J. Phys. Chem. B* 111(27):7812-7824.
20. de Jong DH, Baoukina S, Ingolfsson HI, & Marrink SJ (2016) Martini straight: Boosting performance using a shorter cutoff and GPUs. *Comput. Phys. Commun.* 199:1-7.
21. López CA, Sovova Z, van Eerden FJ, de Vries AH, & Marrink SJ (2013) Martini Force Field Parameters for Glycolipids. *Journal of Chemical Theory and Computation* 9(3):1694-1708.
22. Gu R-X, Ingólfsson HI, de Vries AH, Marrink SJ, & Tieleman DP (2017) Ganglioside-Lipid and Ganglioside-Protein Interactions Revealed by Coarse-Grained and Atomistic Molecular Dynamics Simulations. *J. Phys. Chem. B* 121(15):3262-3275.
23. Vanegas JM, Torres-Sanchez A, & Arroyo M (2014) Importance of Force Decomposition for Local Stress Calculations in Biomembrane Molecular Simulations. *Journal of Chemical Theory and Computation* 10(2):691-702.
24. Goetz R & Lipowsky R (1998) Computer simulations of bilayer membranes: Self-assembly and interfacial tension. *J. Chem. Phys.* 108(17):7397-7409.
25. Admal NC & Tadmor EB (2010) A Unified Interpretation of Stress in Molecular Systems. *J Elasticity* 100(1-2):63-143.

26. Flyvbjerg H & Petersen HG (1989) Error-Estimates on Averages of Correlated Data. *J. Chem. Phys.* 91(1):461-466.